Hot Electron-driven Photocatalysis and Transient Absorption Spectroscopy in Plasmon Resonant Grating Structures

Journal:	*Faraday Discussions*
Manuscript ID	FD-ART-10-2018-000141
Article Type:	Paper
Date Submitted by the Author:	01-Oct-2018
Complete List of Authors:	Cronin, Stephen; University of Southern California, Electrical Engineering; University of Southern California, Physics Wang, Yi; University of Southern California, Electrical Engineering Shen, Lang; Mock Family, Chemical Engineering and Materials Science Hou, Bingya; University of Southern California, Electrical Engineering Poudel, Nirakar; University of Southern California, Electrical Engineering Chen, Jihan; University of Southern California, Electrical Engineering Shi, Haotian; University of Southern California, chemistry Page, William; Ciencia, Inc., Engineering Gibson, George; Ciencia, Inc., Engineering Guignon, Ernest; Ciencia, Inc., Engineering Pilar, Arturo; Ciencia, Inc., Engineering Cady, Nathaniel; SUNY Polytechnic Institute, Colleges of Nanoscale Science & Engineering Dawlaty, Jahan; University of Southern California, Chemistry Wang, Yu; University of Southern California, Electrical Engineering

SCHOLARONE™
Manuscripts

Faraday Discussions

ARTICLE

Hot Electron-driven Photocatalysis and Transient Absorption Spectroscopy in Plasmon Resonant Grating Structures

Received 00th January 20xx,
Accepted 00th January 20xx

DOI: 10.1039/x0xx00000x

www.rsc.org/

Yi Wang,[a,h] Lang Shen,[b,h] Yu Wang,[b] Bingya Hou,[c] George N. Gibson,[e,f] Nirakar Poudel,[c] Jihan Chen,[c] Haotian Shi,[a] Ernest Guignon,[f] Nathaniel C. Cady,[g] William D. Page,[f] Arturo Pilar,[f] Jahan Dawlaty,[a] and Stephen B. Cronin[a,c,d]

Plasmon resonant grating structures provide an effective platform for distinguishing between the effects of plasmon resonant excitation and bulk metal absorption via interband transitions. By simply rotating the polarization of the incident light, we can switch between resonant excitation and non-resonant excitation, while keeping all other parameters of the measurement constant. With light polarized perpendicular to the lines in the grating (i.e., TE-polarization), the photocatalytic reaction rate (i.e., photocurrent) is measured as the angle of the incident laser light is tuned through the resonance with the grating. Here, hot holes photoexcited in the metal are used to drive the oxygen evolution reaction (OER), producing a measurable photocurrent. Using TE-polarized light, we observe sharp peaks in the photocurrent and sharp dips in the photoreflectance at approximately 9° from normal incidence, which corresponds to the conditions under which there is good wavevector matching between the incident light and the lines in the grating. With light polarized parallel to the grating (i.e., TM), we excite the grating structure non-resonantly and there is no angular dependence in the photocurrent or photoreflectance. In order to quantify the lifetime of these hot carriers, we performed transient absorption spectroscopy of these plasmon resonant grating structures. Here, we observe one feature in the spectra corresponding to interband transitions and another featured associated with the plasmon resonant mode in the grating. Both features decay over a time scale of 1-2 psec. The spectral responses of grating structures fabricated with Ag, Al, and Cu are also presented.

Introduction

In the early days of plasmonic catalysis, around 2006, several papers reported photothermally-driven processes, including plasmon resonant chemical vapor deposition (PRCVD).[1, 2] Here, Boyd et al. demonstrated plasmon assisted chemical vapor deposition (PACVD) of PbO nanowires and TiO_2 microstructures by irradiating 23 nm Au nanoaprticles using a metalorganic $Pb(C_{11}H_{19}O_2)_2$ Pb precursor and a $Ti[OCH(CH_3)_2]_2[C_{11}H_{19}O_2]_2$ Ti precursor, respectively.[1] In a similar study, Hung et al. demonstrated plasmon resonant chemical vapor deposition of Fe_2O_3 and carbon nanotubes in CO environment containing trace amounts of iron pentacarbonyl.[2] Here, in situ Raman spectroscopy measurements indicated that temperatures in excess of 1180°C were generated using this approach.

A few years later, around 2010, plasmon resonant enhancement of redox electrochemical processes were demonstrated (including water splitting) by coupling strongly plasmonic metal nanoparticles (e.g., Ag, Au) to strongly catalytic metal oxide semiconductors (e.g., TiO_2).[3-6] Several of these papers have been cited over 500 times, indicating the strong interest amongst the scientific community in plasmon-driven photoelectrochemistry. The initial interpretation of this plasmon resonant enhancement of photoelectrochemical processes was based on local field enhancement of sub-bandgap defect-mediated absorption within the TiO_2 semiconducting material. At this point, large scale electromagnetic simulations using the finite difference time domain (FDTD) method had become commercially available and provided high level of rigor for these nanoscale metal/semiconductor systems. Despite the high degree of accuracy of these electromagnetic simulations, however, several experimental studies reported enhancement factors that were substantially higher than theoretical predictions. For example, Liu et al. reported a 66-fold increase in the photocurrent of a Au/TiO_2 system at a wavelength of 633 nm, which corresponds to photon energy that is roughly half the

[a] Department of Chemistry,
[b] Mock Family Department of Chemical Engineering and Materials Science,
[c] Ming Hsieh Department of Electrical Engineering,
[d] Department of Physics and Astronomy, University of Southern California, Los Angeles, CA 90089, USA
[e] Department of Physics, University of Connecticut, Storrs, CT 06269, USA
[f] Ciencia Inc., East Hartford, CT 06108, USA
[g] SUNY Polytechnic Institute, Colleges of Nanoscale Science & Engineering, Albany, NY 12203, USA
[h] Authors contributed equally.
Electronic Supplementary Information (ESI) available: [details of any supplementary information available should be included here]. See DOI: 10.1039/x0xx00000x

This journal is © The Royal Society of Chemistry 20xx

bandgap of this material, exceeding that which can be explained by simple local field enhancement.[5]

Around 2013, plasmon-induced dissociation of molecular hydrogen was demonstrated in oxide-supported Au nanoparticles in a process that could only be explained by the generation of hot electrons within the metal and subsequent Feshbach resonance.[7, 8] Several theoretical studies ensued calculating the properties of hot electrons in plasmonic nanostructures.[9-11] However, a vast majority of the experimental papers on the subject of hot electron-driven photochemistry entail metal nanostructures in contact with semiconducting material, which presents some additional complexity in the interpretation of charge transfer and energetics, as described above.[12] Park et al. reported hot electron-driven CO oxidation using hybrid metal-semiconductor nanostructures, and reported time-resolved transmission spectroscopy showing hot carrier relaxation on psec times scales.[13] DuChene et al. reported hot hole-driven photoelectrochemical CO_2 reduction using a plasmonic Au/p-GaN photocathode.[14]

In the work presented here, we explore photoelectrochemistry on all-metal nanostructures, which provide a direct means of exploring hot electrons in photoelectrochemical processes. By excluding semiconductor materials from this study, a more straightforward interpretation of data can be achieved regarding behaviour of photoexcited charge in metals. Here, we utilize plasmon resonant gratings to distinguish plasmon resonant excitation from bulk metal absorption via interband transitions. In addition to photoelectrochemical and photoreflectance measurements, we have performed transient absorption spectroscopy in order to establish the time scale over which these hot carriers relax back to equilibrium at the Fermi energy. Electromagnetic simulations of these grating structures using the finite difference time domain method provide a detailed picture of the local field distribution attained under resonant excitation conditions and provide a theoretical estimate for the plasmon resonant enhancement factors in these structures.

Experimental

In this work, we fabricate two types of grating structures. In the first structure, a corrugated surface is first patterned on a silicon substrate with a period of 500 nm using photolithography and reactive ion etching. A 50 nm thick film of Au is then deposited onto this structure, as shown in the SEM image of Figure 1a. Figure 1c shows the reflectance spectrum of one of these grating structures together with that of a bulk Au film. A clear resonance can be seen at a photon energy of 2.0 eV, corresponding to the plasmon resonance of the grating. In a second type of grating structure, we pattern 250 nm thick lines in a Au film with a 500 nm period using photolithography and reactive ion etching, as shown in Figure 6a. The lithography was performed using an ASML deep UV stepper lithography tool. These grating structures were patterned on a transparent BK-7 substrate, which enable transient absorption spectroscopy to be readily performed.

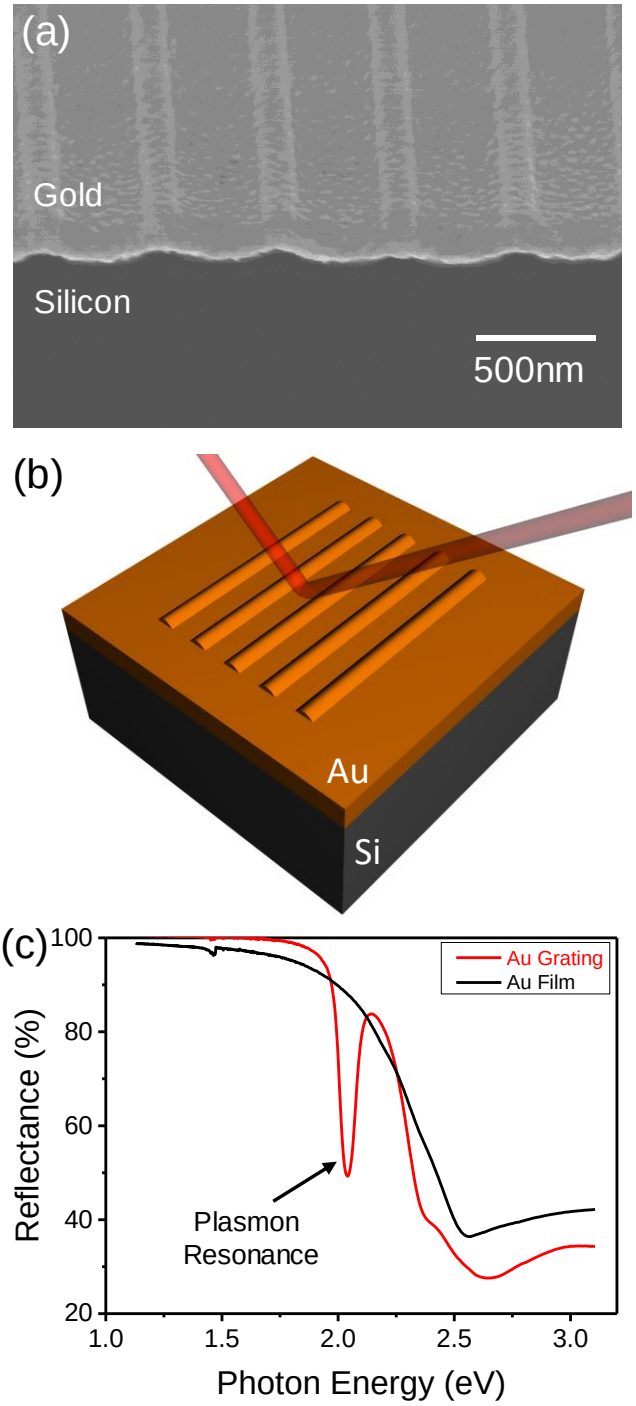

Figure 1. (a) Scanning electron microscope (SEM) image of corrugated Au grating deposited on an underlying silicon substrate. (b) Schematic diagram of these variable angle setup for measuring the photoreflectance and photoelectrochemical current. (c) Photoreflectance spectra for a flat Au film and corrugated grating depicted in (a).

This journal is © The Royal Society of Chemistry 20xx

Photoelectrochemical measurements were performed using a standard 3-terminal potentiostat. In order to measure the small photocurrents associated with the relatively short-lived hot electrons and holes, which are on the order of μA, we use an AC lock-in technique. Here, the incident laser light is modulated using an optical chopper wheel. The current monitor output of the potentiostat is measured by a lock-in amplifier, which is synchronized with the optical chopper, as illustrated in Figure 2a. The grating sample (i.e., working electrode) is mounted on a rotational stage, as illustrated in Figure 2b, which enables us to collect angular dependent photocurrent and photoreflectance spectra. A ½-wave plate is used to rotate the polarization of the incident laser beam. Figure 2c illustrates the hot hole-driven photochemical process in which a hot hole is injected into the solution driving the OER reaction.

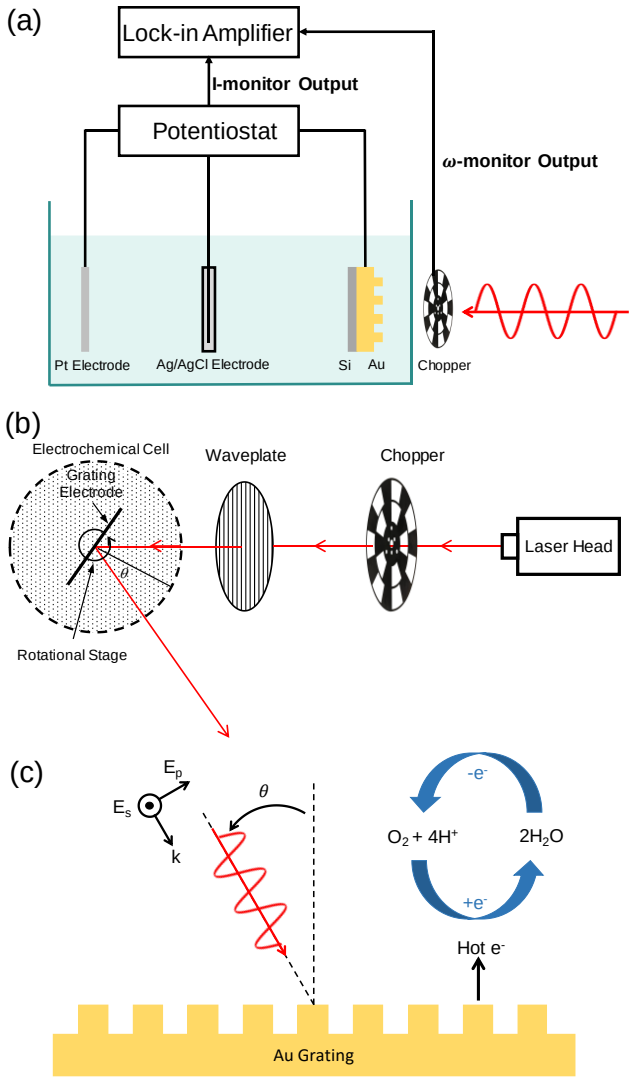

Figure 2. Schematic diagrams for (a) photoelectrochemical setup, (b) angle-dependent photocatalytic measurements, and (c) grating structure for photoelectrochemical setup.

Results and discussion

Before attempting to achieve hot electron-driven photochemistry on plasmon resonant grating structures, we applied the AC lock-in technique depicted in Figure 2a on a 100 nm thick Au film. Here, we are simply exciting the bulk interband transitions in Au without any plasmon resonance.[15] Figure 3 shows the AC photocurrent observed by irradiating this bare Au film using the optically modulated AC lock-in technique in a pH = 7, 0.5M Na_2SO_4 solution. Here, we see a peak in the photocurrent around 1.5V vs NHE. This peak corresponds to the tuning of the relatively narrow distribution of hot holes (illustrated in Figure 3b) through a resonance with the redox potential of the oxygen evolution reaction. These results demonstrate the effectiveness of the AC lock-in technique for measuring photocurrent produced on a bare metal surface for basic water splitting reactions.

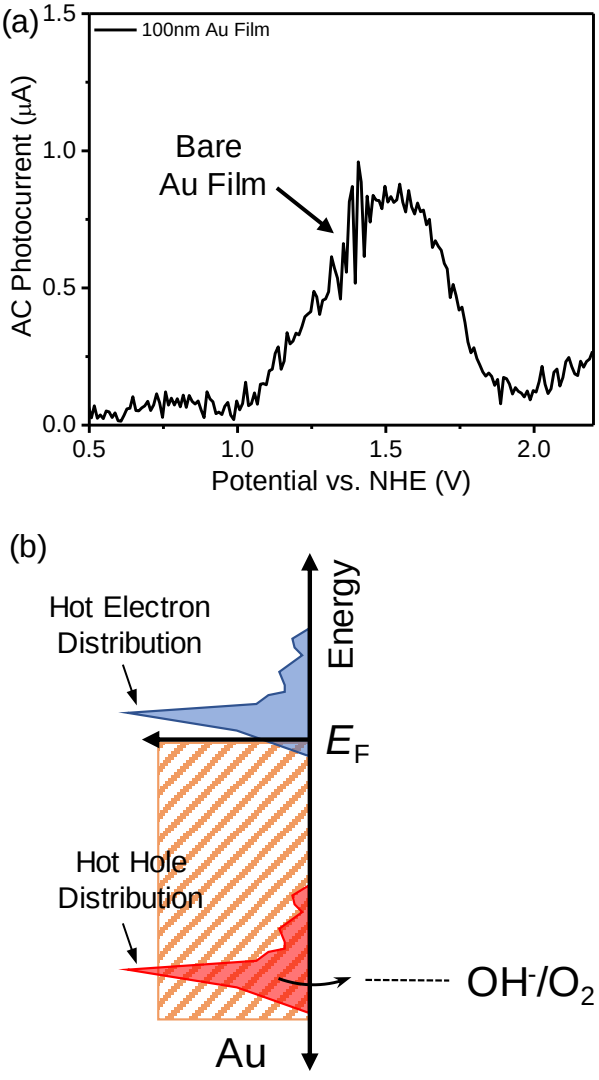

Figure 3. (a) AC Photocurrent measured by irradiating a 100 nm thick gold film in a pH = 7, 0.5M Na_2SO_4 solution with optically modulated 532 nm wavelength light. (b) Energy band diagram indicating the relatively narrow hot electron (blue) and hot hole (red) distributions.

Having demonstrated these capabilities on a bare metal film, we then explored these reactions on plasmon resonant nanostructures in order to amplify this effect. For the plasmon resonant grating structures shown in Figure 1, we have measured the AC photocurrent and photoreflectance as a function of the incident angle. This data, shown in Figure 4, exhibits a sharp peak in the photocurrent as well as a dip in the photoreflectance around an incident angle of 9° from normal incidence. This corresponds to the conditions under which we are resonantly exciting the grating and there is good wavevector matching between the incident light and the lines on the grating. It should be noted that this strong angular dependence of the photocurrent and photoreflectance is only seen when illuminating with TE-polarized light, that is, light polarized perpendicular to the lines on the grating. For TM-polarized light, there is no angle dependence in either the photocurrent or photoreflectance. Here, the non-resonant TM excitation of the metal grating generates a photocurrent of approximately 0.17 μA, due to bulk interband transitions in the Au. These interband transitions have been calculated by Sundararaman, et al. and occur near the L- and X-points in the Brillouin zone.[9] Under resonant excitation with TE-polarized light at an incident angle of 9° from normal incidence, we observe a roughly 2.1-fold increase in the photocurrent due to hot electrons generated in the plasmon resonant mode of the grating. This gain factor is consistent with electromagnetic simulations of these grating structures, as described below in Figure 5.

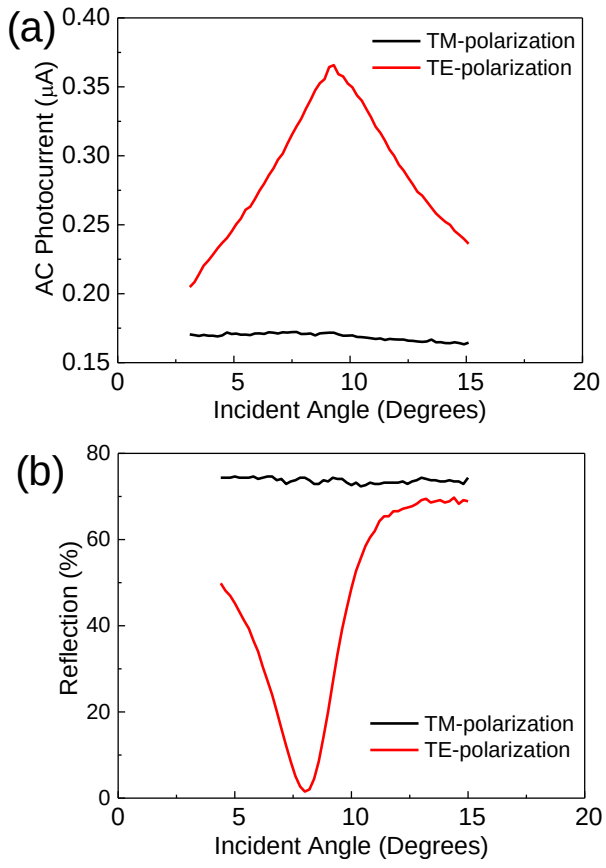

Figure 4. (a) AC Photocurrent and (b) photoreflectance spectra for the 500 nm period Au grating structure shown in Figure 1a plotted as a function of incident angle for both TM- and TE-polarized light.

In order to provide a microscopic picture of the electromagnetic response of these plasmon resonant grating structures, we performed finite difference time domain (FDTD) simulations, which provide the complete electric field and charge distributions of our grating structures under various conditions of excitation both as a function of polarization and incident angle of illumination. Figure 5a shows the calculated photoreflectance plotted as a function of incident angle for both TM- and TE-polarized light. These spectra agree remarkably well with our experimentally observed spectra (plotted in Figure 4b), showing a sharp dip in the photoreflectance at 9° from normal incidence under TE-polarized illumination. Under TM-polarized illumination, the grating simply behaves like a mirror and exhibits no angular dependence. The electric field intensity distributions calculated at 9° incidence are plotted in Figures 5b and 5c for the TM- and TE-polarizations, respectively. Here, the electric field intensity is plotted on the colour scale indicated on the side of the Figure. This is a linear scale corresponding to the multiplicative factor of enhancement with respect to the incident electric field intensity of the incident light. For the case of resonant excitation with TE-polarized light, the peak field intensity (corresponding to red on this scale) is approximately 18 times higher than the incident electric field intensity. Under TM-polarized excitation, shown in Figure 4b, no field enhancement is achieved, and a vast majority of the incident photons are simply reflected off the metal surface along with a small amount of bulk Au interband absorption, as described above. Based on these FDTD simulations, we can estimate a plasmonic enhancement factor based on the following equation:

$$EF = \frac{\int_{f(x,y)-10\text{nm}}^{f(x,y)} |E_{\text{TE}}|^2 dxdydz}{\int_{f(x,y)-10\text{nm}}^{f(x,y)} |E_{\text{TM}}|^2 dxdydz}$$

where E_{TE} and E_{TM} are the electric field strengths under TE-polarized and TM-polarized illumination, respectively. Here, we integrate over the corrugated surface topography f(x,y) from the surface of the Au grating, indicated by the dashed lines in the Figure, down 10 nm below the surface, corresponding roughly to the hot electron diffusion length. Upon performing this integral, we obtain a theoretical plasmon resonant enhancement factor of 15.9X. This is considerably higher than the enhancement observed experimentally, indicating that significant losses occur as these hot electrons/holes are transferred to the ions in solution.[16] These losses are not accounted for in these simulations.

This journal is © The Royal Society of Chemistry 20xx

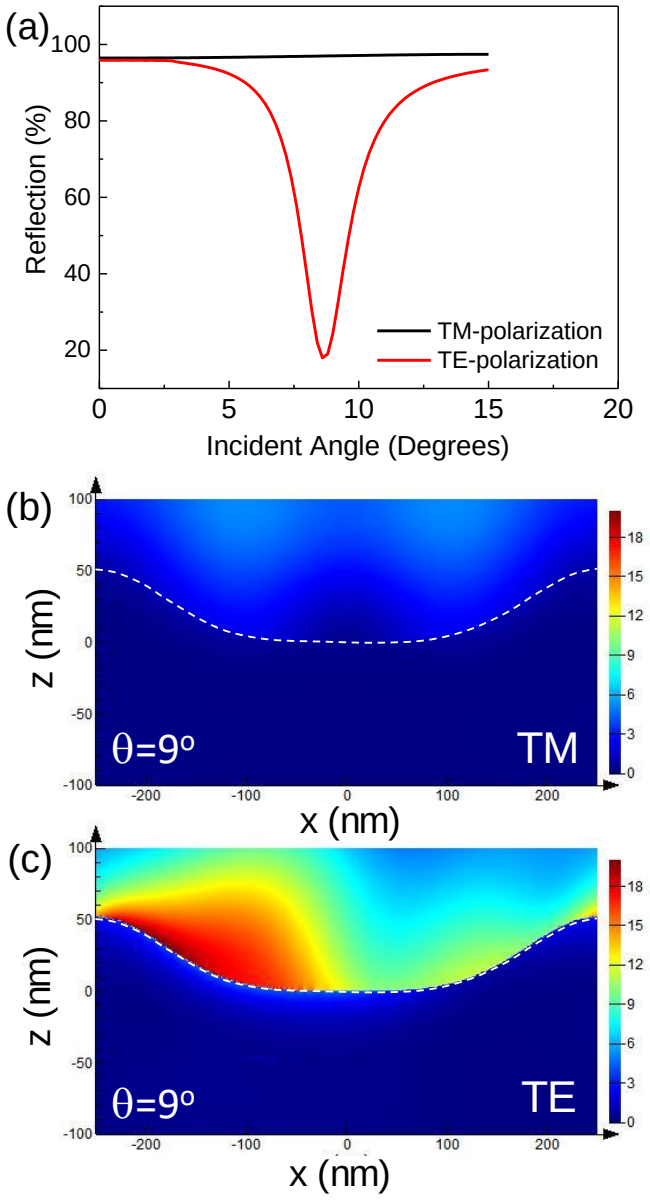

Figure 5. (a) Calculated photoreflectance spectra for the 500 nm period grating shown in Figure 1a for both TM- and TE-polarized light. Electric field intensity distributions calculated at an incident angle of 9o from surface normal for (b) TM-polarized and (c) TE-polarized light. Here, the Au/water interface is indicated by the white dashed lines.

One of the open questions in the field of hot electrons is how long these optically-excited hot carriers live in metals, and to what extent their energy and charge can be harvested before they decay back to equilibrium at the Fermi energy. In order to address this open question, we performed transient absorption spectroscopy (TAS). This is a pump-probe technique, in which a 50 fsec pump pulse is first used to optically excite hot electrons and hot holes in the material, and then broadband absorption spectra are collected as a function of time. Since this technique requires transparent samples, we used optically transparent gratings shown in Figure 6 consisting of 300 nm wide lines with a 500 nm period patterned into a 50 nm thick Au film on a BK-7 substrate using reactive ion etching. The UV-vis abortion spectrum is shown in Figure 6b, which exhibits a resonant feature around 550 nm.

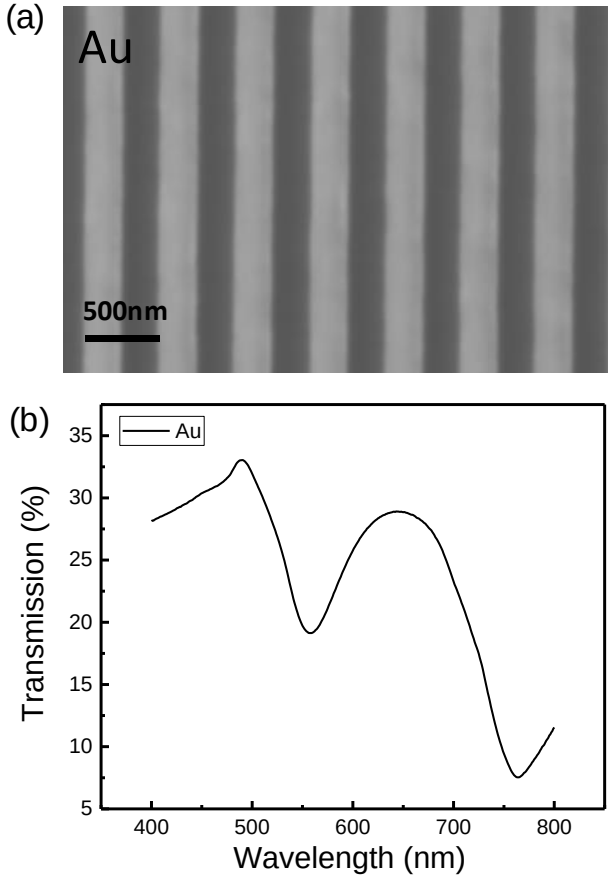

Figure 6. (a) SEM image and (b) UV-vis transmission spectrum of a Au grating with a 250 nm line width and 500 nm period.

The transient absorption spectra of these plasmon resonant grating structures are plotted for both the TM-polarized, non-resonant excitation (Figure 7a) and TE-polarized, resonant excitation (Figure 7b). Here, the pump wavelength is approximately 560 nm and the broadband absorption spectra are collected over a wavelength range from 400 nm to 600 nm. For non-resonant, TM-polarized excitation, we see one dominant feature in these spectra around corresponding to interband transitions within the bulk Au material. These interband hot carrier excitations decay over a time scale of 1-2 psec. It is, in fact, these interband transitions that give rise to gold's yellow colour. Figures 7c and 7d show the electric field distributions of similar grating structures illuminated with TM- and TE-polarized light, respectively. When illuminated on resonance with TE-polarized light, the local electric fields are enhanced by roughly a factor of 10. However, it should be noted that these local fields, and hence the hot electron-hole pair generation, are confined within the top few nanometers of the gold surface, which is advantageous for photocatalysis, since it is difficult for these hot electrons and holes to diffuse over long distances in metals without relaxing back to

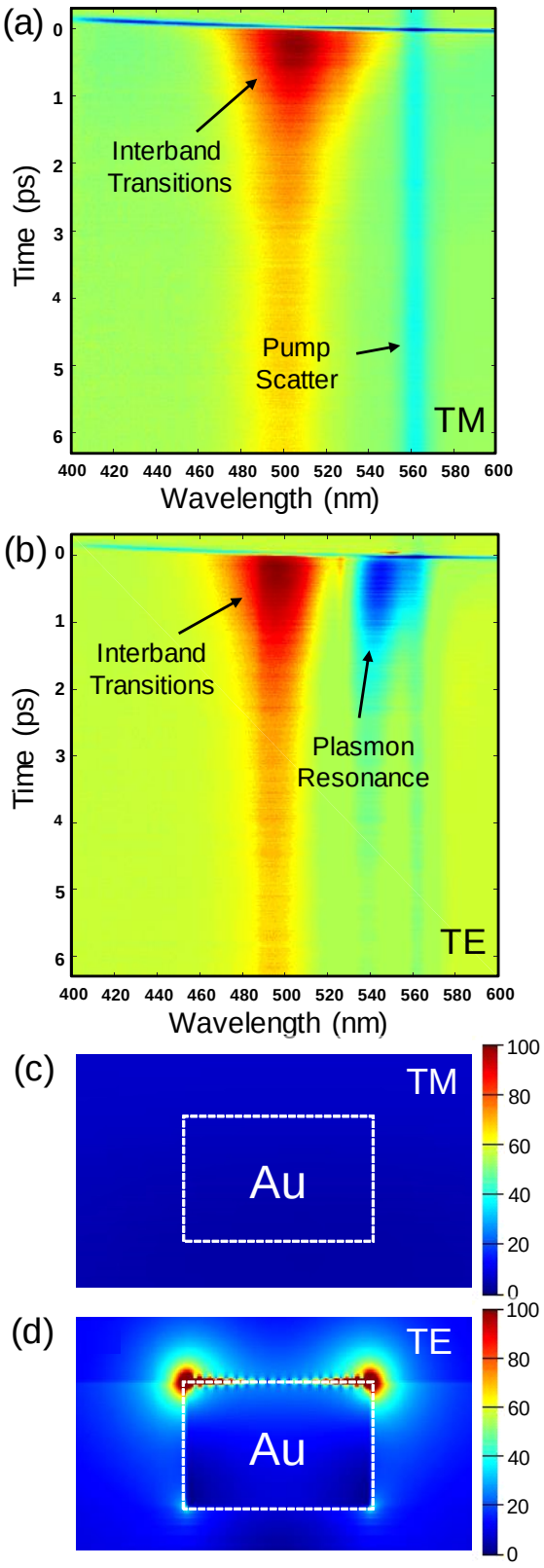

Figure 7. Transient absorption spectra of the Au grating structure shown in Figure 6 taken with (a) TM-polarized and (b) TE-polarized light. (c,d) Electromagnetic simulations plotting the cross-sectional electric field intensity distributions of grating structures illuminated with TE-polarized and TM-polarized light.

equilibrium. Figure 7b shows the transient absorption spectra of the resonantly excited grating structure under TE-polarized illumination. These spectra were obtained under the same conditions as those in Figure 7a, the only change being the rotated polarization of the incident light. Here, we see the same feature at 500 nm corresponding to the interband transitions in bulk Au, which decay over a time scale of 1-2 psec. In addition to this interband transition feature, however, we also see the emergence of a new feature at 540 nm, which corresponds to the plasmon resonant mode of the grating structure. The photo-excited hot carriers associated with this plasmon resonance also decays over a time scale of 1-2 psec. Here, the plasmon resonance gives rise to ground state bleaching, which makes this feature appear as a negative change in transmission (ΔT/T). After the Au is excited by the pump laser, there are fewer plasmon electrons in the pumped sample and more electrons in the excited states than the non-pumped sample. Since the transient absorption spectrum is a result of pumped probe minus non-pumped probe, therefore the plasmon resonance peak appears to be negative. Upon closer inspection, one can notice a slight time-dependent blueshift of this plasmon resonant mode. This aspect of the data enables us to further distinguish these two absorption mechanisms. More specifically, the plasmon resonant absorption peak blueshifts with time possibly due to the change in refractive index caused by injected carriers in the surrounding medium or to an optical Kerr effect, which is exacerbated by local field enhancement of the plasmon resonant mode and not present in bulk interband absorption. This blueshift may provide additional insight into the nonlinear response of hot electrons in metals and charge transfer in this system. Similar blueshifts have been reported in TiO_2-supported Au nanoparticle systems.[17]

Based on our FDTD simulations, we can predict the behaviour of grating structures consisting of different metals such as Ag, Al, and Cu. Figure 8a shows the simulated photoreflectance spectra of the same corrugated grating structures shown in Figure 1 calculated with Au, Ag, Al, and Cu. Based on these calculations, we expect Ag to produce a narrower resonance than Au and at slightly lower incident angles than Au. Similarly, we expect Al to produce a narrower resonance than Ag and at a lower incident angle than Ag. Figures 8b-8d shows the experimentally measured angular dependent photoreflectance spectra of the corrugated gratings fabricated with Au, Ag, and Al taken with both TM- and TE-polarized light. Here, we see qualitative agreement with the prediction of the FDTD calculations. Namely, the Ag resonance is narrower than Au and occurs at a lower incident angle than Au. Also, the Al resonance occurs a lower incident angle that Ag, however, its lineshape is not in fact narrower than that of Ag.

This journal is © The Royal Society of Chemistry 20xx

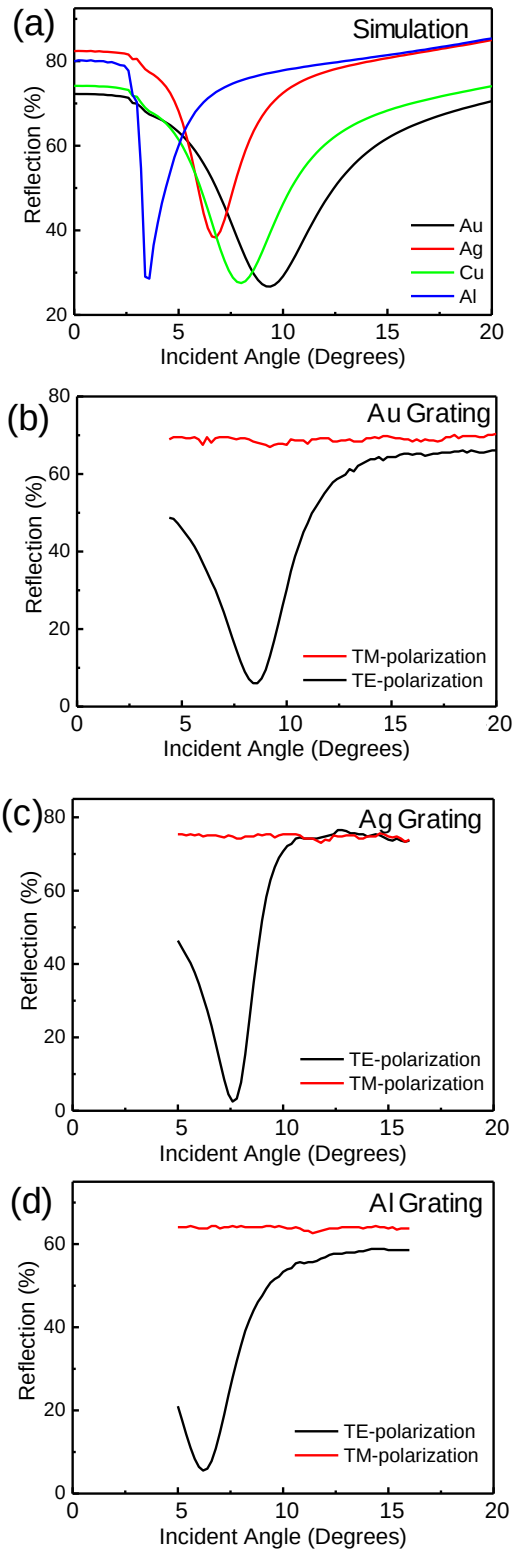

Figure 8. (a) Calculated photoreflectance spectra of Au, Ag, Cu, and Al gratings with geometry depicted in Figure 1a. Experimentally measured photoreflectance spectra of (b) Au, (c) Ag, and (d) Al gratings taken with both TE- and TM-polarized light.

We have also evaluated the spectral response of the semi-transparent grating structures (similar to those used in the transient absorption measurements) for Al, Ag, and Cu metals. Figure 9 shows SEM images and UV-vis spectra of these Au, Ag, Al, and Cu gratings. It should be noted that the lithographic processing of the Ag gratings did not work well because of the chemical sensitivity of Ag, which readily forms an oxide that is soluble in water. In order to achieve the 200-300 nm feature sizes using photolithography, an anti-reflective coating is deposited on top of the Ag surface. As one of the last steps in the processing, a reactive ion etch is used to remove this anti-reflective coating. Unfortunately, however, this etch step oxidized the Ag and then partially dissolved the material, as is readily apparent in the SEM image of Figure 9. Despite this poor quality, the spectral response of the Ag is still somewhat sharp, as evident in the UV-vis spectrum shown in Figure 9. The grating peaks for the Cu are not as apparent because of the strong interband transitions in this metal, which give rise to its reddish colour.

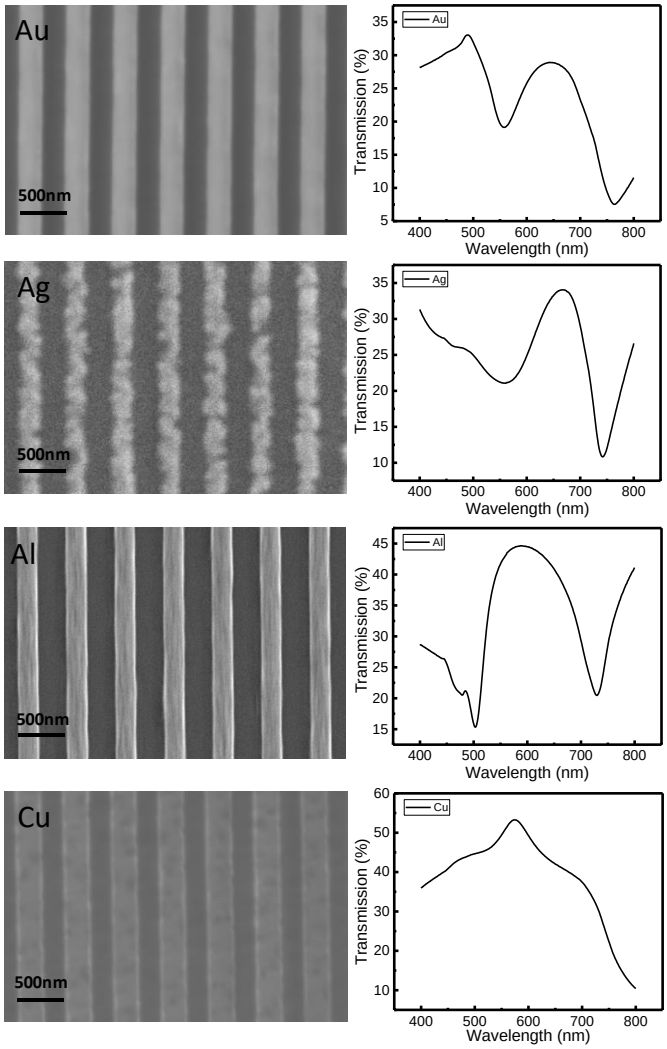

Figure 9. SEM images and UV-vis transmission spectra of semi-transparent Au, Ag, Al, and Cu gratings.

Conclusions

In conclusion, we have developed a method for measuring the relatively small photocurrents produced by hot electrons and holes that are photoexcited in bulk metal films. By patterning these metals into plasmon resonant grating structures, we demonstrate enhanced photoelectrochemical performance in these hot-electron/hole mediated processes. The plasmon resonant grating structures enable us to compare interband absorption and plasmon resonant excitation by simply rotating the polarization of the incident light, while leaving all other parameters of the measurement constant. At a fixed laser wavelength, we can tune through the plasmon resonance of the grating. Sharp peaks in the photoelectrochemical current (i.e., reaction rate) and corresponding dips in the photoreflectance of the grating are observed around 9^o from normal incidence. Under non-resonant photoexcitation, we explore photocatalysis driven by bulk metal interband absorption. Under resonant excitation, we explore photocatalysis driven by surface plasmon modes, which are largely confined to the first few nanometers of the Au surface. Transient absorption spectroscopy performed under resonant and non-resonant conditions reveal that there are two mechanisms of photoexcitation of hot electrons/holes. Both the non-resonant excitation of interband transitions in the bulk Au material and the plasmon resonant mode relax back to equilibrium over a timescale of 1-2 psec. In addition to being spectrally distinct, the plasmon resonant mode produces a negative change in the optical transmission ($\Delta T/T<0$) and exhibits a time-dependent blueshift associated with the local enhanced fields of the plasmon mode. In addition to Au, gratings fabricated with Ag and Al exhibit similar spectral features presenting additional promising platforms for hot electron and hot hole drive photocatalysis.

Conflicts of interest

There are no conflicts to declare.

Acknowledgements

This research was supported by ARO Award No. W911NF-17-1-0325 (Yi W.), the U.S. Department of Energy, Office of Science, Office of Basic Energy Sciences, under Award DE-SC0019322 (Yu W.), NSF Award No. CBET-1512505 (L.S.), AFOSR Grant No. FA9550-15-1-0184 (B.H.), DOE Award No.DE-FG02-07ER46376 (N.P.), ACS-PRF Grand No. 55993-ND5 (J.C.), and ARO Award No. W911NF-14-1-0228 (H.S.).

Notes and references

1. Boyd, D.A., L. Greengard, M. Brongersma, M.Y. El-Naggar and D.G. Goodwin, *Plasmon-assisted chemical vapor deposition.* Nano letters, **6**, 2592-2597 (2006).

2. Hung, W.H., I.-K. Hsu, A. Bushmaker, R. Kumar, J. Theiss and S.B. Cronin, *Laser directed growth of carbon-based nanostructures by plasmon resonant chemical vapor deposition.* Nano letters, **8**, 3278-3282 (2008).

3. Christopher, P., H. Xin and S. Linic, *Visible-light-enhanced catalytic oxidation reactions on plasmonic silver nanostructures.* Nat Chem, **3**, 467-72 (2011).

4. Ingram, D.B., P. Christopher, J.L. Bauer and S. Linic, *Predictive Model for the Design of Plasmonic Metal/Semiconductor Composite Photocatalysts.* ACS Catalysis, **1**, 1441-1447 (2011).

5. Liu, Z., W. Hou, P. Pavaskar, M. Aykol and S.B. Cronin, *Plasmon resonant enhancement of photocatalytic water splitting under visible illumination.* Nano Lett, **11**, 1111-6 (2011).

6. Ingram, D.B. and S. Linic, *Water splitting on composite plasmonic-metal/semiconductor photoelectrodes: evidence for selective plasmon-induced formation of charge carriers near the semiconductor surface.* J Am Chem Soc, **133**, 5202-5 (2011).

7. Mukherjee, S., F. Libisch, N. Large, O. Neumann, L.V. Brown, J. Cheng, J.B. Lassiter, E.A. Carter, P. Nordlander and N.J. Halas, *Hot electrons do the impossible: plasmon-induced dissociation of H2 on Au.* Nano Lett, **13**, 240-7 (2013).

8. Mukherjee, S., L. Zhou, A.M. Goodman, N. Large, C. Ayala-Orozco, Y. Zhang, P. Nordlander and N.J. Halas, *Hot-electron-induced dissociation of H2 on gold nanoparticles supported on SiO2.* J Am Chem Soc, **136**, 64-7 (2014).

9. Sundararaman, R., P. Narang, A.S. Jermyn, W.A. Goddard, 3rd and H.A. Atwater, *Theoretical predictions for hot-carrier generation from surface plasmon decay.* Nat Commun, **5**, 5788 (2014).

10. Brown, A.M., R. Sundararaman, P. Narang, W.A. Goddard, 3rd and H.A. Atwater, *Nonradiative Plasmon Decay and Hot Carrier Dynamics: Effects of Phonons, Surfaces, and Geometry.* ACS Nano, **10**, 957-66 (2016).

11. Narang, P., R. Sundararaman and H.A. Atwater, *Plasmonic hot carrier dynamics in solid-state and chemical systems for energy conversion.* Nanophotonics, **5** (2016).

12. Kim, S.M., S.W. Lee, S.Y. Moon and J.Y. Park, *The effect of hot electrons and surface plasmons on heterogeneous catalysis.* J Phys Condens Matter, **28**, 254002 (2016).

13. Park, J.Y., S.M. Kim, H. Lee and Nedrygailov, II, *Hot-electron-mediated surface chemistry: toward electronic control of catalytic activity.* Acc Chem Res, **48**, 2475-83 (2015).

14. DuChene, J.S., G. Tagliabue, A.J. Welch, W.H. Cheng and H.A. Atwater, *Hot Hole Collection and Photoelectrochemical CO2 Reduction with Plasmonic Au/p-GaN Photocathodes.* Nano Lett, **18**, 2545-2550 (2018).

15. Hou, B., L. Shen, H. Shi, R. Kapadia and S.B. Cronin, *Hot electron-driven photocatalytic water splitting.* Phys Chem Chem Phys, **19**, 2877-2881 (2017).

16. Shen, L., G.N. Gibson, N. Poudel, B. Hou, J. Chen, H. Shi, E. Guignon, N.C. Cady, W.D. Page and A. Pilar, *Plasmon resonant amplification of hot electron-driven photocatalysis.* Applied Physics Letters, **113**, 113104 (2018).

17. Aiboushev, A., F. Gostev, I. Shelaev, A. Kostrov, A. Kanaev, L. Museur, M. Traore, O. Sarkisov and V. Nadtochenko, *Spectral properties of the surface plasmon resonance and electron injection from gold nanoparticles to TiO2 mesoporous film: femtosecond study.* Photochemical & Photobiological Sciences, **12**, 631-637 (2013).

 This journal is © The Royal Society of Chemistry 20xx